Received: 15 July 2024 | Accepted: 26 October 2024

DOI: 10.1111/mice.13376

RESEARCH ARTICLE

COMPUTER-AIDED CIVIL AND INFRASTRUCTURE ENGINEERING WILEY

A dynamic neural network model for the identification of asbestos roofings in hyperspectral images covering a large regional area

Donatella Gubiani[1] | **Giovanni Sgrazzutti**[1] | **Massimiliano Basso**[1] | **Elena Viero**[1] | **Denis Tavaris**[2] | **Gian Luca Foresti**[2] | **Ivan Scagnetto**[2]

[1]Services and Systems for Environment, Territory and Agriculture, Insiel Spa, Udine, Italy

[2]Department of Mathematics, Computer Science and Physics, University of Udine, Udine, Italy

Correspondence
Department of Mathematics, Computer Science and Physics, University of Udine, Ivan Scagnetto, Via delle Scienze, 206, Udine, 33100, Italy.
Email: ivan.scagnetto@uniud.it

Abstract

Asbestos has been used extensively in several applications. Once it is known as a dangerous mineral, its usage has been prohibited and its identification and remediation play a very important role from the health safety point of view. Nowadays, deep learning techniques are used in many applications, especially for image analysis. They can be used to significantly reduce the time and cost of traditional detection methods. In this paper, taking advantage of asbestos spectral signature, a deep neural network is introduced in order to implement a complete methodology to identify asbestos roofings starting from hyperspectral images in a regional context. The novelty of the proposed approach is a dynamic mixing of models with different features, in order to accommodate classifications on widespread areas of both urban and rural territories. Indeed, the dataset used during the experiments described in this paper is a large one, consisting of many wide hyperspectral images with a geometric resolution of 1 m and with 186 bands, covering an entire region of approximately 8,000 km^2. This is in contrast to other works in the literature where the analyzed areas are limited in size and uniform for physical features.

1 | INTRODUCTION

The main purpose of this work is to propose a general methodology to detect the presence of asbestos in roofings, analyzing airborne acquired hyperspectral images. The detection works both at the raster level (per pixel) and at the vector level (GIS tools), in order to assess asbestos materials in buildings.

Asbestos fibers have exceptional resistance to heat, fire, and chemical agents; moreover, they have low thermal and electrical conductivity, and materials containing asbestos show high mechanical resistance. Hence, they have been extensively used in the past in several industrial applications, the most popular being asbestos roofs.

However, asbestos is also known as a dangerous mineral fiber causing serious health hazards to those who are exposed to it. As a consequence, the necessity to remove asbestos from legacy buildings is also compelled by common regulations in several countries. For instance, in Italy there is a plethora of laws and regulations about asbestos since 1992 (Camera dei Deputati, 2022). Such rules are then implemented at a local level in all Italian regions, for example, in Friuli Venezia Giulia (FVG for short, the region where the experiments described in this paper

have been carried out) there is a strict legislation (Regione Autonoma Friuli Venezia Giulia, 2023). Moreover, at a higher level, in the European Union (EU), in order to better safeguard the health of workers, the European Parliament and the Council have recently approved Directive (EU) 2023/2668 (amending the previous Directive 2009/148/EC in a substantial way). Such directive, dated November 22, 2023 and currently effective, sets a control limit for asbestos at 0.01 fibers per cubic centimeter of air (0.01 f/mL), which is 10 times lower than previously. EU member countries now have 2 years (i.e., by December 20, 2025) to fully implement the directive.

Hence, it is critical to detect asbestos-containing materials (ACMs) accurately and in time in order to ensure public safety and to execute efficient asbestos treatment methods. Traditional asbestos detection procedures, such as direct inspections on site and sample analysis are often time-consuming, labor-intensive, expensive, and limited in scope. To address these issues, scientists have resorted to new technologies to improve the efficiency and accuracy of asbestos detection.

Hyperspectral imagery (HSI) is an advanced remote sensing technique capturing detailed spectral information for each pixel in an image. In computer vision, it enhances object recognition and classification by revealing specific spectral characteristics, enabling the detection of subtle differences and aiding in the identification of indistinguishable materials/objects. In our case, since the high number of spectral bands in HSI, the spectral signature that characterize asbestos can be used to distinguished it from other materials.

These applications can benefit from recent developments in the research field of deep neural networks (DNNs) applied to computer vision. Indeed, DNNs, a subset of artificial intelligence and machine learning, have demonstrated outstanding performance in a variety of image processing applications. These models excel at learning patterns and representations from complex data, making them perfect for dealing with asbestos detection challenges. DNNs may learn to recognize ACMs with high precision and generalization by training them on huge datasets of tagged images and can represent a preliminary step to guide more focused field inspections and laboratory analysis.

In this paper, a large and significant case study is described about detecting asbestos roofs by applying DNNs to high-resolution hyperspectral images. Indeed, the underlying research goal is to use deep learning techniques in conjunction with spectral data to produce an accurate and efficient approach for identifying ACMs in building roofings. As it will be shown in later sections, the network's learnt features and capabilities will be used in differentiating asbestos-related materials by fine-tuning a custom network using the dataset of the Autonomous Region Friuli Venezia Giulia, which has been accurately analyzed and annotated for asbestos identification. The effectiveness of the developed DNN for asbestos detection is evaluated using an on-map validation. In addition, the limitations of the proposed methodology and some related potential future work directions will be highlighted.

In Section 2, other asbestos detection approaches in the literature are discussed. Sections 3 and 4 describe the data used in the experiments and the proposed methodology, respectively. Then, Section 5 shows the carried out experiments and, finally, conclusions and further works are discussed in Section 6.

2 | RELATED WORK

Several studies concerning mapping roofing with ACMs have been proposed in the literature. In this context, to our knowledge, the most complete critical survey of the state-of-the-art methods is proposed in Abbasi et al. (2022). The authors review studies proposed from 2012 to 2022 and summarize them according to the input imagery types and image classification processes.

2.1 | Input imagery types

Hyperspectral imagery. Due to the rich spectral information of HSI, it has been widely utilized as a reliable data source in order to classify roofs containing asbestos by the correspondent spectral wave (Cilia et al., 2015; Szabó et al., 2014; Fiumi et al., 2012, 2014; Frassy et al., 2014). Nevertheless, despite the advantages of HSI, certain limitations exist. Specifically, the high dimensionality can negatively impact the classification process (Szabó et al., 2014; Hamedianfar et al., 2014): conventional classification algorithms typically do not perform well with high-dimensional data. Therefore, selecting bands and determining an optimal resolution become critical tasks in the process (Hughes, 1968; Kavzoglu & Mather, 2002; Hountondji et al., 2006).

Multispectral imagery/panchromatic images. Considering that spatial resolution is often more advantageous than spectral resolution when extracting features such as ACM roofs (Neupane et al., 2021), other studies have explored the use of multispectral imagery (MSI) or panchromatic images (de Pinho et al., 2012; Gibril et al., 2017; Tommasini et al., 2019; Taherzadeh & Shafri, 2013; Abriha et al., 2018), which have fewer bands compared to HSI, but more than classical RGB images (Raczko et al., 2022; Krówczyńska et al., 2020). Moreover, contrary to the past, MSI now provides extremely high resolutions, is typically more

affordable, and covers larger areas. In some instances, MSI is also combined with LiDAR (Norman et al., 2020).

2.2 | Image classification processes

As far as the processing algorithms are concerned, different kind of solutions to detect ACM roofings have been used in the literature.

Spectral angle mapper. The spectral angle mapper algorithm is really common to solve this task. It is a pixel-based approach; indeed, the algorithm evaluates the similarity between spectral signatures by calculating the angle between the spectrum under investigation and the reference spectrum, in the n-dimensional space of the bands (Marino et al., 2001; Fiumi et al., 2012, 2014; Szabó et al., 2014; Frassy et al., 2014; Cilia et al., 2015; Krówczyńska et al., 2016).

Maximum likelihood classifications. The maximum likelihood classifications differently define the reference classes for each band so that their statistics follow a Gaussian distribution. The probability that each pixel has of belonging to a given class is then determined (Szabó et al., 2014; Taherzadeh & Shafri, 2013).

Segmented pixels (objects) algorithms. However, as remarked before, improvements of remote sensing imagery resolution, have forced researchers to consider alternative solutions with respect to per-pixel spectral-based approaches, at least for classifying asbestos roofs. The underlying observation is that per-pixel-based approaches combined with traditional classifiers can lead to unreliable classifications of images, due to the increasing intraclass variability of classes with high-resolution data. In Myint et al. (2011), the authors show that when using high-resolution sensors it is common to observe different features (e.g., roofs) on the surface of the Earth that are made up of materials having comparable spectral responses. Whence, a plethora of other algorithms segment images and use segmented pixels (called objects) as units to process, taking into account both spatial and spectral features (Hay & Castilla, 2008; Blaschke et al., 2014; Navulur, 2006). Objects are handled by developing a number of rules for classifying features such as texture, size, and geometry (de Pinho et al., 2012).

Support vector machines. Among the most advanced traditional techniques, there is the support vector machines (SVM), a supervised classification model belonging to kernel-based methods, which allows a mapping of the dataset from the features space to an higher dimensional kernel (Szabó et al., 2014; Hamedianfar et al., 2014; Hamedianfar & Shafri, 2014; Norman et al., 2020; Gibril et al., 2017). SVM, in particular, does not require an estimate of the statistical distributions of the various classes but defines the classification model by exploiting the concept of maximizing the margins between the classes.

Random forests. The random forest, on the other hand, is based on the use of decision trees (DTs) associated with a criterion of purity of the indices: alongside a series of sequential tests to separate the samples to obtain more or less pure classes, various classifiers are used, built on training data and creating, from time to time, DTs based on the tests, assuming the one that receives the most votes as the most reliable solution (Gibril et al., 2017; Tommasini et al., 2019; Abriha et al., 2018; Hamedianfar et al., 2014; Norman et al., 2020).

Neural networks. Finally, DNNs have achieved admirable performance in a large number of applications. In particular, convolutional neural network (CNN) models are popularly and successfully in computer vision for object detection, segmentation etc., even in problematic scenarios, for example, in underwater environments (Foresti & Scagnetto, 2022), in emotional state analysis (Olamat et al., 2022), in brain disorders detection (Ozdemir et al., 2021), etc. The versatility of CNNs and convolutions in general goes beyond the computer vision field, allowing researchers to build models and applications in other scenarios. For instance, in Duchesne et al. (2013), the authors develop a survival analysis model to predict the overall structural state of a sewer network. Other examples are graph convolutional networks (GCNs), that is, models where convolutions operate on graph-structured data. Remarkable applications of GCNs are used, for instance, in civil infrastructures contexts, supporting optimal repair decisions for, for example, water distribution networks (Fan et al., 2022).

Moreover, in recent years, CNNs produced state-of-the-art results for pixel classification in HSI. The main reason of their success relies upon the fact that the majority of these methods examine both spatial and spectral channels to extract features for classification, avoiding the accuracy issues mentioned before. For instance, in Sarma and Kakarla (2022), the authors propose a CNN which has been tested on the publicly available HSI datasets with good results.

In Kakarla (2020), the second author of Sarma and Kakarla (2022) published an implementation of a DNN tested on the Pavia University dataset (Gamba, 2023). Taking advantage of the open source Keras library, he implemented his proposal in the Python language and showed how the network works on the single Pavia University hyperspectral image, whose main features are the following ones: 103 spectral bands, 610×340 pixels, resolution 1.3 m. Compared to the proposal in Sarma and Kakarla (2022), the network has a different architecture (without convolutions and with only 89,574 total parameters against the 2,460,065 parameters), but the accuracy results on the

same dataset seem to be comparable. It includes 12 fully connected or dense layers, two batch normalization layers, and two dropout layers to yield a land cover classification. Such model distinguishes between nine classes (asphalt, bare soil, bitumen, gravel, meadows, painted metal sheets, self-blocking bricks, shadows, and trees). Since also in the case discussed in this paper there is a dataset of urban areas hyperspectral images, such architecture has been taken into consideration, with the required variations and integrations. Indeed, our dataset encompasses a very wide geographic area, covered by a huge number of images with a considerable variation of their features. All details are described in the following sections (in particular in Section 3), with specific considerations also introducing the proposed methodology (Section 4), and describing the experiments (Section 5). Moreover, the distinguishing aspects of the approach presented in this work rely on an integrated methodology where the architecture of the underlying DNN is not so important by itself, but as a tool to generate a mixing of three models. In particular, while the first two models are trained on global data, the third one is trained dynamically on data similar to those of the area to be processed. This allows to take into account peculiar features of the candidate area which may not be considered enough by the other two models.

3 | DATA

In the following, the HSI dataset used throughout the experiments will be introduced and illustrated in Section 5. Differently from other HSI datasets publicly available on the Internet and usually employed in published works (see, e.g., those used in Sarma and Kakarla, 2022) which refer to a single image with a limited landscape, the proposed dataset is really a huge one. It consists of more than 4000 hyperspectral images of approximately 5000 × 2500 pixels with 186 bands, and a spatial resolution of 1 m (approximately 10 GB/image).

3.1 | Hyperspectral images

The regional hyperspectral survey was carried out in two subsequent phases: initially, only the Province of Trieste was acquired (the dataset was named *Lotto Giuliano*); at a later stage, the rest of the region was taken over (the dataset was named *Lotto Unico*). This work focuses on the images of the latter dataset, which covers 95% of the regional territory of FVG (which totally amounts to 7924 km^2).

The hyperspectral images were acquired via a HySpex VNIR 1800 sensor fixed on an aircraft at a flight altitude of approximately 3000 m. At this height, the sensor guaranteed a final pixel spatial resolution of 1.0 m. The acquisition of the stripes was adapted according to the conditions and morphological characteristics of the surveyed area (e.g., plain or mountain area) and the planning of the stripes provided for a lateral overlap of approximately 30%, in order to guarantee a contiguous coverage even in the presence of turbulence or sudden changes in the platform's attitude.

The hyperspectral data are available partitioned by acquisition stripe both in "original" format, corresponding to the length of the single flight path (Figure 1a), and in "reduced" form, by cutting the original stripes onto a unit length of approximately 5000 m (Figure 1b).

Each hyperspectral image is available as a file in .bsq (band sequential raster) format, a standard format that allows simple sequential management and storage of raster data. Alongside the .bsq, the information relating to the georeferencing of the image, number of bands, pixel dimensions, etc. is contained within a related .hdr file. A raster image of this format can be displayed in any GIS software (e.g., QGIS; https://www.qgis.org), by selecting the triplet of 186 bands useful for video display. Figure 1b shows an example.

3.2 | Asbestos data

Starting from the previously described hyperspectral images, a first identification of asbestos roofings in the regional territory was carried out. The processing, commissioned to an external company, involved 24 municipalities in the area of *Lotto Unico* and integrated also ad hoc local surveys carried out with a drone.

Such activity yielded as a result a vector layer (shape format) containing the polygons related to the ACM roofs identified in each of the 24 examined municipalities (red layer in Figure 1c), in addition to the frames of the drone flights. Each polygon is accompanied by a series of descriptive attributes, including the asbestos status and the uncertainty level.

3.3 | Building roofings

Several information layers relating to existing buildings are available from IRDAT.[1] Among these, it is possible to have the buildings of the CTRN.[2] For instance, Figure 1c (black

[1] The Regional Environmental and Territorial Data Infrastructure; in Italian known as "*Infrastruttura Regionale dei Dati Ambientali e Territoriali (IRDAT)*" at https://www.regione.fvg.it/rafvg/cms/RAFVG/ambiente-territorio/conoscere-ambiente-territorio/FOGLIA2/ (May 20, 2024).
[2] The Technical cartography of the FVG Region available in scales 1:5,000 and 1:10,000; in Italian: "*Carta Tecnica Regionale Numerica (CTRN)*."

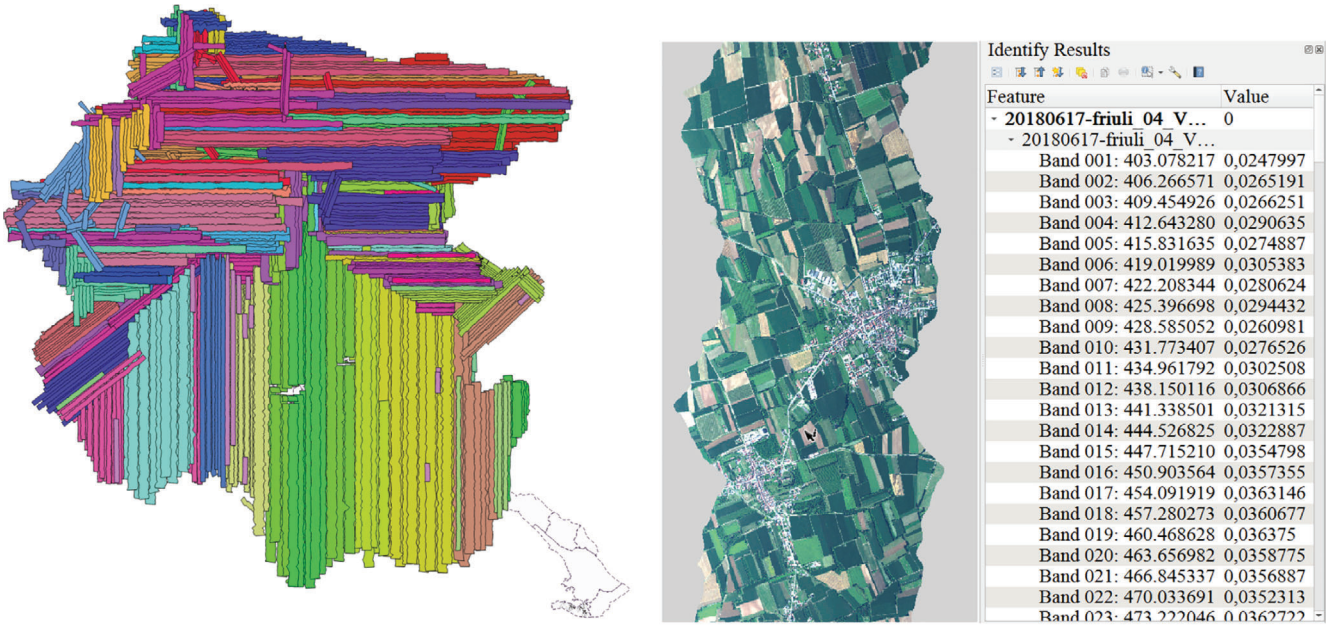

(a) Partition of the hyperspectral survey according to the acquisition stripes (the colors refer to the specific acquisition date).

(b) An extracted image of the hyperspectral relief with true color RGB bands and some examples of reflectance values associated with the selected pixel (QGIS tool).

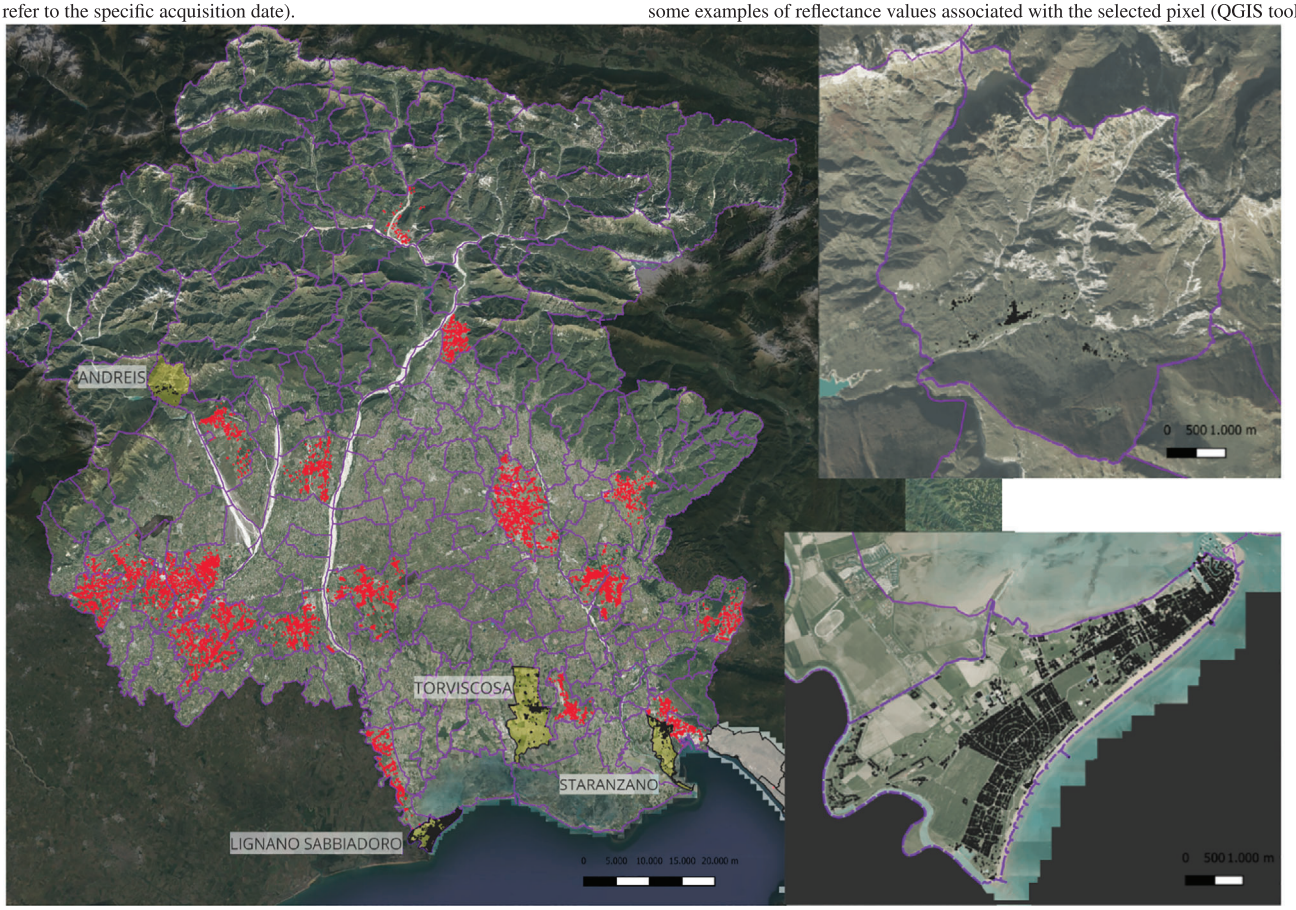

(c) On the left, Regional map showing data of the first identification of asbestos roofings of 24 Municipalities (red) and the 4 Municipalities involved in the experimentation (yellow) with buildings (black). On the right, zoom on the Municipalities of Andreis and Lignano Sabbiadoro with CTRN buildings (black).

FIGURE 1 Available hyperspectral data.

layer) shows the CTRN buildings of the municipalities considered in our experiments.

Regulations regarding asbestos were introduced in FVG and throughout Italy with Law No. 257 of 1992. At the regional level, the Regional Asbestos Plan[3] was implemented in 1996 and is periodically updated. Since a version of the data from the CTRN produced in the 1990s is available, it can reasonably be assumed that no asbestos-cement coverings have been installed after that period. Therefore, it can be assumed that the buildings represented in this version of the CTRN contain all potentially detectable asbestos coverings and can thus be used as a filter to isolate the data to be analyzed for our purposes.

4 | METHODOLOGY

The work proposed in Kakarla (2020) is a good starting point. However, since its approach cannot be directly applied to the context taken into consideration, several modifications and integrations were carried out, in order to deal with our large dataset and to correctly identify asbestos roofings.

Indeed, the large set of hyperspectral images includes more than 4,000 images to cover the entire Region FVG (about 7900 km^2) with a resolution of 1 m. Each image has about 5000 × 2500 pixels organized in different ways (vertical, horizontal, or oblique), each one associated with 186 bands, for approximately 10 GB/image. The georeferencing and temporal resolution of the images play a relevant role. The images are georeferenced (RDN2008/UTM zone 33N (N-E), EPSG:6708) and spatial location is relevant both for combining different images, which have about 30% of overlap, and for connecting to buildings. For temporal resolution, due to the spatial extension of the region, surveys have been carried out on different days and hours, with different flight directions, light and weather conditions that influence band values. A more extended list of features is summarized in Table 1.

Moreover, our goal is not a simple supervised classification, but the identification of asbestos pixels, in order to detect asbestos roofings. The final result cannot be a mere raster map but has to be postprocessed to obtain a final vector layer that includes polygons representing asbestos roofing of buildings.

Starting from these considerations, the proposed methodology is based on two successive steps as resumed graphically in Figure 2. The first step works at the raster level. It is based on a neural network that returns raster classification maps (Section 4.1). The second step passes from the raster level to the vector one. It combines classification maps with the building vector layer and returns a vector layer with buildings identified with asbestos roofings (Section 4.2).

[3] In Italian: "*Piano Regionale Amianto (PRA)*."

TABLE 1 Features of hyperspectral images (Lotto Unico).

Feature	Description
Format files	`.bsq` + `.hdr`
Number of bands	186
Band format	Decimal
Spatial resolution	1 m
Dimension of images	About 5000 × 2500 pixels organized in different ways (vertical, horizontal, or oblique)
Size of images	About 10 GB/image
Number of images	More than 4000
Spatial extension	Images covering almost the entire region Friuli Venezia Giulia about 7900 km^2 divided into plains, hills, and mountains
Temporal resolution	Different by day and flight hours
Additional features	Georeferenced and overlapped images, presence of pixel no-data

4.1 | The first step: A neural network for a raster classification

Starting from several preliminary analyses carried out on various ground truth datasets, it is clear that many models differ quite a lot in making predictions. In particular, some models are either more or less "generous" than others in terms of identifying asbestos class pixels; moreover, the pixels belonging to buildings recognized as asbestos by a greater number of models actually corresponded to real asbestos coverings. Building upon these observations, it was decided to opt for the use of a combined solution that compares the results of predictions based on different models against each other.

Hence, the first phase of raster data processing was structured into the following steps:

1. Training multiple models and making predictions with them, yielding raster images for each prediction (for each processed image);
2. Combining different predictions, yielding a "final" raster image obtained from the integration of the single predictions (for each processed image).

The proposed network, adapted from the one made available in Kakarla (2020), is implemented in Python using the open-source library KERAS (https://keras.io) for machine learning and neural networks. Therefore, it

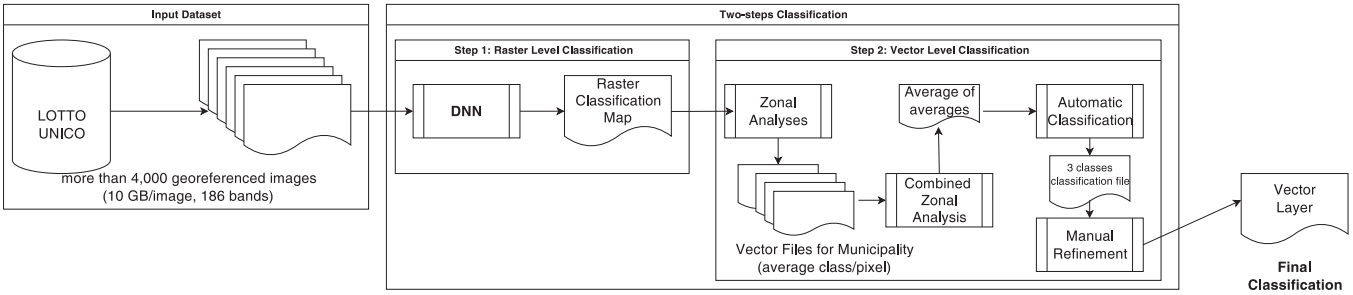

FIGURE 2 Methodology of input preprocessing and classification.

was possible to extend and integrate the available code to achieve the desired results. The main implemented aspects can be summarized as follows:

- The use of the libraries `SPECTRAL.IO.ENVI` and `RASTERIO` allowed the management of hyperspectral images in `.bsq`/`.hdr` format and the georeferencing of the classification maps returned by the network;
- specific functions were implemented to work on subsets of pixels (rectangular matrices of variable size), according to the specific sampling needs of the ground truth, stored in `.h5` format (using the `H5PY` library), and then combined in different ways, according to the different needs;
- processing functions for image strip bands (250/1,000 rows of pixels, depending on the type of strip) were implemented to avoid overloading memory and to compute multiple models in the shortest possible time, reducing the number of image-loading operations.

4.2 | The second step: From raster classification to building roofings

Due to the need of identifying asbestos roofings based on raster results obtained from different processed models, the second step of the proposed methodology focuses on the considered buildings and allows the transition from raster maps obtained during the first phase to a final vector result that identifies buildings with asbestos roofings.

The second phase of processing is therefore focused on the vector layer of buildings and consists of the following steps:

1. Zonal analysis: For each prediction, vector files are created for the entire municipality under examination and there is the computation of the average asbestos/nonasbestos class value (1/0) of the pixels contained in each individual building.
2. Combination of different zonal analyses: A vector file is created for the entire municipality, and it is derived from joining the various files obtained in the previous step and computing the average of the averages.
3. Automatic classification: The previous file is extended with an attribute of automatic classification into three classes (nonasbestos, unclear/doubtful, asbestos), whose value is determined based on thresholds defined on the averages of each individual prediction and on the average of the averages.
4. Manual refinement in postprocessing: The results of automatic classification are checked, allowing to possibly modify the classification.

The automatable steps of the second phase of the methodology have also been implemented in Python, working in this case in the QGIS environment (https://www.qgis.org).

The last point, which is not automatable, in this phase makes use of the GIS tools leveraging available maps, and, in particular, of the true orthophoto available at the regional level with a resolution of 10 cm (related to a survey in the years 2017–2020), and of the potential availability of images from Google StreetView. With this processing, the aim is to verify unclear/doubtful cases and to obtain a classification of coverings at the vector level that includes the following classes: nonasbestos, likely nonasbestos, unclear/doubtful, likely asbestos, and asbestos.

5 | EXPERIMENTS

As mentioned before, the experiments focused on the area covered by the "Lotto Unico," which encompasses over 95% of the regional territory and includes data related to asbestos detection previously acquired in 24 municipalities.

Four municipalities (yellow ones in the left map in Figure 1c) have been involved during this experimental phase. They all are characterized by rather different features:

TABLE 2 Properties of municipalities.

Municipalities	Area (m^2)	Buildings (m^2)	Density (%)
Andreis	26,880,823	47,941	0.18
Lignano Sabbiadoro	15,623,500	1,339,710	8.57
Staranzano	18,464,945	390,409	2.11
Torviscosa	48,152,322	460,622	0.95
	109,121,590	2,238,682	2.05

- Andreis (detailed map in the upper right in Figure 1c) is a mountain municipality in the west area of the FVG region: it is a small town surrounded by an extended area without buildings;
- Lignano Sabbiadoro (detailed map in the bottom right in Figure 1c) is a tourist municipality in the extreme southwest of the region, located on a horizontal peninsula facing south on the upper Adriatic Sea and north on the Marano lagoon. It does not have a very large area but has a high density of buildings with respect to other considered municipalities;
- Torviscosa is a municipality located at the center of the lower Friulian plain;
- Staranzano is a municipality located in the southeast zone of the region, at the right of the Isonzo river mouth, overlooking the sea, but full of green areas.

The dimensions of the four municipalities in terms of territorial and built area is summarized in the left columns of Table 2.

All the experiments have been performed on a machine with the following configuration, running the Linux Ubuntu 22.04 operating system:

- Dual Xeon 2678 V3 CPUs, with a total number of 24 cores/48 threads,
- 128 GB RAM,
- 1 TB SSD storage,
- three dedicated graphics cards Nvidia GTX 1080 Ti with 11 GB RAM each.

Due to the large amount of images to handle, a workspace on a 10 TB network drive was also used.

5.1 | Classes and ground truth assessment

The first experiments were carried out with a classification scheme similar to that proposed in Kakarla (2020). There was not a comprehensive class set, but the activity was focused on distinguishing the presence of asbestos from different types of roofings. Thus, a classification with six classes was initially defined, including

1. asbestos,
2. vegetation (grasslands, trees, forests, fields, areas with vegetation, etc.),
3. asphalt (anthropogenic elements outside buildings, such as roads, sidewalks, parking lots, etc.),
4. red coverings (red roofings),
5. non-red roofings (gray and other roofings, no red or asbestos),
6. no-data, considering the presence of no-data pixels as visible in Figure 1b, each image includes two external zones where data are not available and to combine different images these areas have to be recognized.)

As shown in Figure 3a,b, for the assessment of the ground truth, rectangular subareas were identified within the available strips (at least one for each of the 24 municipalities for which we had data from the previous identification of asbestos roofings), identifying areas where asbestos was present in higher quantities. Each individual asbestos polygon, excluding uncertain cases, was verified and manually adjusted to avoid including "dirty" pixels in the training dataset by checking hyperspectral images displayed through RGB bands. We remark that the selection and analysis of the training and test areas was made on all the municipalities where a greater presence of asbestos was highlighted (examples in Figure 3a).

Notice that an automatic generation of the ground truth assessment was not possible for several reasons. First, the hyperspectral images are not truly orthorectified; therefore, they may present significant deviations from the polygons corresponding to asbestos roofings (especially when they are at a certain height). Additionally, the presence of vegetation or different artifacts covering the roofs, even partially, would have "contaminated" the training set.

Similarly, polygons corresponding to the other considered classes were in turn identified. The vector data of the ground truth in different areas was rasterized and prepared for subsequent use in the training phase.

The classification actually used for the final processing was not the one described so far, but an automatic reorganization into only three classes:

1. asbestos;
2. non-asbestos (class including all extra-asbestos);
3. no-data.

However, the classification into six classes was crucial for the control and cleaning of the assessment of the ground truth. Indeed, through the analysis of spectral signatures for each class, a series of pixels presenting

(a) Example of a rectangular area used to assess the ground truth.

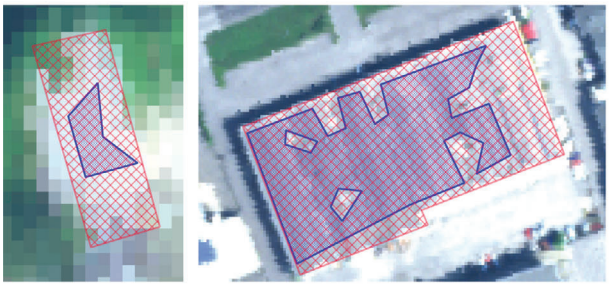

(b) Two examples of asbestos roof with the corresponding polygon selection.

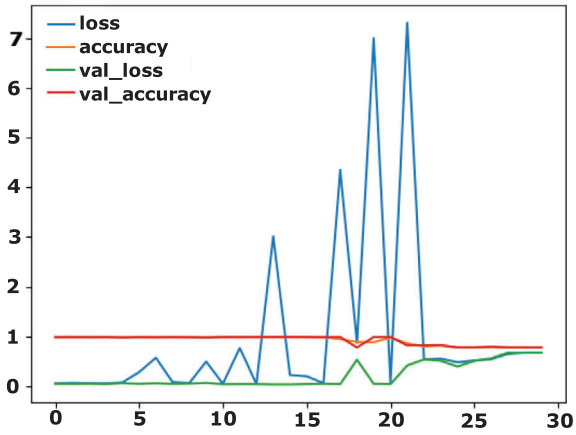

(c) Training trend during epochs with 3 classes and data of 24 municipalities.

	precision	recall	f1-score	support
1. asbestos	0.87	0.95	0.91	22237
2. vegetation	1.00	0.98	0.99	72241
3. asphalt	0.88	0.72	0.79	11239
4. red roofs	0.99	0.72	0.84	8368
5. non-red roofs	0.53	0.76	0.62	8854
6. noData	1.00	1.00	1.00	28557
accuracy			0.93	151496
macro avg	0.88	0.85	0.86	151496
weighted avg	0.94	0.93	0.94	151496

	precision	recall	f1-score	support
1. asbestos	0.92	0.93	0.93	23835
2. non-asbestos	0.98	0.98	0.98	99104
noData	1.00	1.00	1.00	28557
accuracy			0.98	151496
macro avg	0.97	0.97	0.97	151496
weighted avg	0.98	0.98	0.98	151496

(d) Results on test data: classification with 6 classes on the left, classification with 3 classes on the right.

FIGURE 3 Training and test.

problems (burned pixels on some bands) or not respecting the spectral signature associated with the corresponding class were identified and excluded from the ground truth.

The overall ground truth assessed upon the 24 municipalities is given by a set of 7,148,809 pixels (+ no-data) of which 614,924 pixels belong to the asbestos class.

5.2 | Neural network and classification maps

For the processing of the first phase of the proposed methodology, several trainings and tests were carried out on different subsets of the ground truth previously

assessed for the 24 municipalities for which there was available asbestos data. In any case, the ground truth data were split into a training set and a test set with a ratio of 70/30.

5.2.1 | Training and test of the neural network

The base neural network, as implemented in Kakarla (2020), has 12 fully connected or dense layers, two batch normalization layers, and two dropout layers. In our case, working with 186 bands, there is a total number of 100,431 parameters (100,059 parameters are trainable).

The model uses rectified linear unit as activation function, categorical cross entropy as loss function, and the chosen optimizer is the Adam optimization algorithm. Indeed, the latter is known to have many benefits, for example, computational efficiency and being well suited for problems with many data and/or parameters (as in the case of hyperspectral images). Accuracy is used as a metric, and there are two callbacks for early stopping (when there is no improvement), and for saving model/weights at some interval, in order to continue the training later from the saved state.

The trainings have shown good levels of accuracy already from the early epochs of execution. For instance, the first epoch of training in the case of the three classes on the data of the 24 municipalities highlighted the following results:

Train: `loss: 0.0558 - accuracy: 0.9800` and
Validation: `loss: 0.0419 - accuracy: 0.9841`.

Such results improved during the next 15 epochs, as depicted in Figure 3c, yielding the following:

Train: `loss: 0.2221 - accuracy: 0.9841` and
Validation: `loss: 0.0300 - accuracy: 0.9878`.

In the training phase, a high number of epochs was set but never reached due to the implementation of "early stopping" (set to 15 epochs), which stops the training after a certain number of epochs without improvements. This indicates how the abundance of information available through the 186 available bands allows for a good discrimination among the considered classes. Notice that this also implies that the training loss values oscillate a lot even when the model converges to high values of accuracy, since the network must adapt its weights to new inputs (never seen before). Hence, if such inputs are "similar" to previous ones the train loss will be low, otherwise there can be even high spikes like in the mentioned figure (loss: blue curve).

The initial tests, useful for understanding the neural network's functioning on the examined data, focused on the area of the Municipalities of Udine and San Giovanni al Natisone. Subsequently, they expanded to the areas of the Municipalities of Azzano Decimo and Fiume Veneto to verify the combination of ground truths derived from flights carried out on different dates and over more distant territories (over 50 km). The training dataset was then gradually expanded until reaching the entire ground truth created for the 24 available municipalities.

It is worth noticing that the original algorithm, which inspired this work, was applied to a single hyperspectral image of relatively small dimensions (less than 0.5 km^2), and the data were "uniform" within it. Conversely, in the present case, the analyses covered a much larger surface area, with significant territorial differences from one area to another. These differences were further highlighted by the fact that the flights were performed on different dates, with different times, lighting conditions, and weather conditions.

From the several tests carried out, it became evident that extending the training set generally led to a slight reduction in the network's performance, both in terms of validation and particularly at the testing level. In any case, the models trained on the 24 municipalities showed an overall accuracy on validation of 97–98%. It decreases during the tests but anyway, in particular for the three-class model, it remains over 92% (as visible in Figure 3d). Furthermore, upon analyzing the data related to the asbestos class (our main interest), such as the general accuracy parameter, even the values of precision, recall, and F1-score appear to have better values in the case of the three-class model (Figure 3d right side), compared to the six-class model[4] (Figure 3d left side). This observation was made across various training tests, and therefore, the subsequent processing was focused on the three-class models. The six-class classification was eventually used to verify specific situations.

In addition, another ground truth of smaller dimension was created. Although it referred to the same 24 municipalities for which the previous asbestos identification was known, it was acquired on different areas with respect to those used previously. The tests carried out on this ground truth (on which pixel cleaning was not performed, but issues were present in a very limited number) yielded generally slightly lower results with respect to those on validation on the previous data, varying depending on the training dataset.

As expected, the closer the training dataset is to these data, the better the results. For this reason, a methodology

[4] This observation occurred after the identification and cleaning of pixels that showed issues within the ground truth.

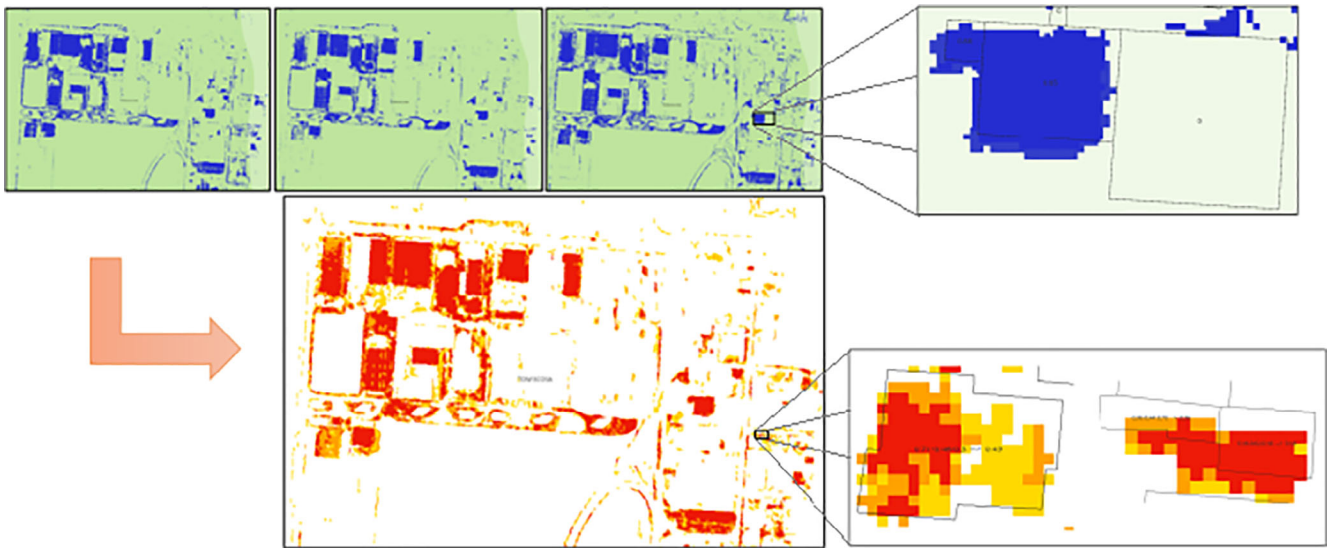

FIGURE 4 Comparison between three models: an example about the classification maps related to an industrial area (left) with some details combined with the vector layer (right).

based on the use of different training/models was developed, one of which was specifically chosen with characteristics closest to the municipality under examination: same flights, same days, or at least with similar territorial characteristics.

In order to process each municipality in a thorough way, the network was trained on different datasets, yielding three different models, according to the selection made on the training sets:

- total training (data from 24 municipalities);
- partial training (data from four municipalities, where preliminary tests were carried out and on which good results were verified);
- adapted training (data from municipalities close to or "similar to" the municipality under investigation).

For instance, the example area shown in Figure 4 refers to the case of the Municipality of Torviscosa. In this case, the adapted model was created starting from the ground truth data available for the Municipalities of Tavagnacco, Udine, and Pradamano with whom it shared flights and whose strips cover a large part of the municipal territory (same days, fairly uniform time slots, and predictably similar weather conditions).

As it is shown in Figure 4, in the upper part of the image, the classifications obtained starting from the three different training sessions are in general quite similar to each other (the same consideration also applies to the other municipalities considered, albeit with minor differences from case to case). Starting from these results, a map is created, assigning colors to the pixels based on the number of models that identify each specific pixel as asbestos:

0. no model identifies the pixel as asbestos (white);
1. only one of the models identifies the pixel as asbestos (yellow);
2. two out of three models identify the pixel as asbestos (orange);
3. all three models identify the pixel as asbestos (red).

As visible in the bottom part of Figure 4, there is a the prevalence of white pixels, that is, identified as asbestos by none of the models, and red pixels, that is identified as asbestos by all three models.

5.3 | From raster to buildings

Zonal analysis is a classic operation of the GIS environment: it allows one to calculate the statistics of a raster layer for each element of an overlapping polygonal vector layer. In our specific case, this allowed us to connect the individual classification maps to the polygons available within the buildings layer at our disposal.

In particular, during the experiments the calculation of the average of the values of the asbestos/nonasbestos (Boolean map) has been carried out within each individual building, in relation to each individual classification. The averages obviously take a value between 0 and 1, where 0 indicates that no pixel belonging to the geometry was recognized as asbestos and 1 indicates that all pixels were recognized as asbestos. For intermediate values, however, the following occurs: the closer the value is to 0, the less likely the presence of asbestos is, the closer the value is to 1, the more likely the presence of asbestos is. The result of this processing is available in a vector layer

where each building has associated the average of each single model and their average as visible in some examples in Figure 4.

In particular, in the example on the right-top with a single model, three buildings are visible and one can see how the two buildings on the left, almost completely covered by pixels recognized as asbestos (blue pixels), have associated an average value close to 1, while the building on the right with no pixels recognized as asbestos has an average of 0. In the examples on the right-bottom, it is instead visible how the combination of the different classifications has a different effect on the averages.

In all the cases shown in the right examples in Figure 4, it is also possible to see how the non-true orthorectification of the images leads to a certain deviation between the polygons of the building and the corresponding pixels in the classification which obviously has different effects depending on the situation. This highlights how the processing must take into account a certain level of imprecision in order to identify buildings with asbestos roofing. These were fundamental observations towards the definition of thresholds able to automatically produce an automatic classification between buildings with asbestos or non-asbestos roofing.

On the basis of checks and tests on statistical data for single and combined classification, two conditions with respective thresholds were identified which made it possible to automatically distinguish in a first step between buildings with asbestos and non-asbestos roofs:

- non-asbestos roofings have a relatively low asbestos pixel count:
  - single models: mean < 0.1;
  - combination of models: mean < 0.33;
- asbestos roofings have a relatively high asbestos pixel count:
  - single models: mean > 0.6;
  - combination of models: mean > 0.83.

The automatic classification thus defined has already made it possible to obtain a good discrimination between asbestos situations (from 1% to 8% of buildings depending on the municipality considered) and non-asbestos situations (from 84% to 96% of buildings). Only a portion ranging from 3% to 10% of the buildings considered, based on the municipality analyzed, remained outside the conditions previously described and was assessed as a doubtful case. This fact reduces more than 10 times the effort/time of a complete check on all buildings.

Starting from these doubtful cases, but carrying out more general checks on the different situations, a series of inspections was carried out with the support of GIS tools through the use of hyperspectral images, regional RGB orthophotos and, where possible, with verification on Google StreetView images.

This "manual" analysis made it possible to confirm many of the roofings identified as asbestos (an example in Figure 5a) and not asbestos. It also highlighted particular situations that required manual interventions on the data:

- roofs partially covered by vegetation (examples in Figure 5a,b): due to the part hidden by vegetation it was not possible to correctly classify the asbestos automatically. However, if a part of the coverage is visible and identified by the classification, through a visual check on the map, manual intervention can correct the classification (Figure 5b);
- buildings with different roofs in which one part is clearly identified as asbestos and one is not (examples in Figure 5a,b): the building is represented in the vector layer as a single polygon but has different roofs or appears to be an aggregate of different buildings. Given the clear distinction at the classification map level, a visual check on the map allows one to verify these situations. In this case, a partitioning of the original polygon is required for correct classification (Figure 5b);
- false positives (an example in Figure 5b): in some cases, the spectral signature of asbestos can be confused with that of spectrally similar materials (such as the case of fiber cement) and only an in-depth analysis in the field by experts in the sector can allow the resolution of such situations;
- in some cases, asbestos roofs have already been removed and are therefore no longer detectable. In these cases, if the building no longer exists, it is excluded from the results.

5.4 | Results

Table 3 shows the results obtained from the processing. Assuming that the role of the operator can influence the results and that the final classification requires a more detailed investigation on the territory by experts, the final check using GIS tools allowed us to carry out a first level of verification of the results that can be defined positive.

Although it was not possible to verify several situations because they were not visible or could not be assessed by eye, in general 45% of the doubts and unclear situations could be resolved and some other cases could be confirmed or modified.

Comparing the accuracy parameters of the different trained models, the identified asbestos seems to be higher than the real asbestos roofs. However, this is not a problem in our context, since the proposed methodology allows to

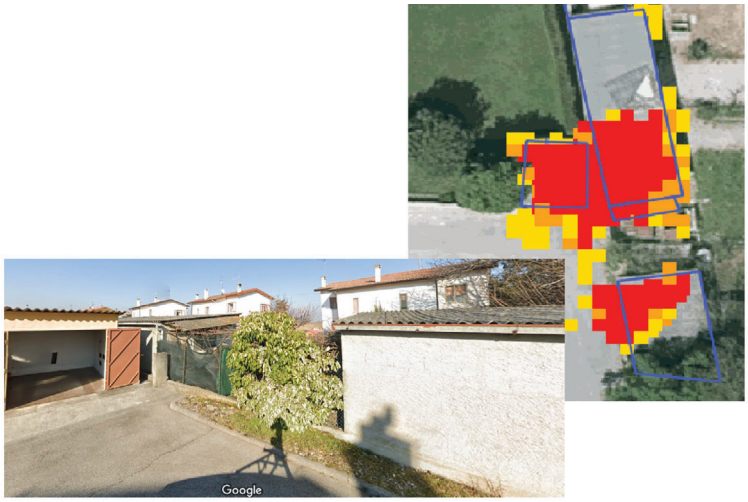

(a) Example with different situations verified in Google Street View: a) building on the left correctly recognized with asbestos roofing b) long building at the top indicated as doubtful as one half is clearly identified as asbestos while the other is not c) building at the bottom doubtful as it is partially covered by vegetation.

(b) Three particular situations: 1. a building with asbestos roofing partially covered by vegetation; 2. a building polygon representing three distinct roofs and for which partitioning is required; 3. a residential building recognized as asbestos but which at first sight does not appear to be.

FIGURE 5 Examples of roofs partially covered by vegetation.

TABLE 3 Summary of results.

Automatic classification		Modifications (%)					Final classification	
Classes	**Roofs**	**Andreis**	**Lignano S.**	**Staranzano**	**Torviscosa**	**Total**	**Roofs**	**Classes**
Asbestos	685	0	34	12	3	**20**	541	Asbestos
							145	Likely asbestos
Doubt	1,486	33	50	40	29	**45**	874	Doubt
No asbestos	15,025	1	2	30	26	**10**	590	Unlikely asbestos
							15,098	No asbestos
	17,196	2	6	5	5	6	17,248	

drastically reduce the number of buildings/roofs to check, in order to focus the investigations on the whole territory. With our experiment, starting from a set of 17,196 buildings and focusing on roofs classified as asbestos, likely asbestos or doubt, the initial set can be reduced to 2171 buildings (less than 13%) automatically and to 1560 buildings (about 9%) after the manual check on the map.

On the other side, even if only part of the roof is visible in the hyperspectral images, the manual check on the map can also identify specific situations where vegetation

covers roofs or errors in the building layer. In addition to the doubtful cases, some of the above-mentioned cases (with vegetation coverings) can be identified in buildings that are automatically identified as no-asbestos and, therefore, changed to doubtful or probable asbestos.

Moreover, the municipality of Lignano Sabbiadoro shows the highest number of manual modifications on roofs automatically identified as asbestos (34%) and doubtful (50%). This may be due to three main aspects: (i) the high presence of buildings (generally also of a certain age) compared to the other municipalities considered, (ii) the large pine forest covering many buildings, and, probably, (iii) the effect of sand and pine needles spreading everywhere and interfering with the values detected by the hyperspectral instrument.

6 | CONCLUSION

Our work had the goal of experimenting the use of a DNN for the classification of hyperspectral images, in order to identify and map the asbestos-cement roofings existing in some municipalities of the Region FVG in Italy.

Starting from a neural network used for other purposes and made available by Kakarla (2020), the appropriate code additions were carried out to adapt the algorithm to the available hyperspectral data. Thanks to the help of specific open-source libraries, it was possible to manage the network until acquiring a certain level of knowledge of the results proposed by the output predictions. An engineering of the image processing pipeline was applied: starting from the hyperspectral raster data and the analysis of the spectral signatures, then passing through the manual classification and training phase, up to the execution of the network prediction itself, and to the vectorization and postprocessing phases.

The main novelty is the proposed methodology which leverages on three models to carry out the classification (in the specific case, this amounts to detect asbestos roofings). In particular, the technique of combining a model trained on a partial initial dataset (with good verified results) with a model trained on the whole dataset, and an adaptive model related to areas similar to that under investigation allowed an accurate classification of a wide territory with different features. According to our knowledge, there are not so widespread experiments in the scientific literature about HSI datasets.

Indeed, comparing the results depicted in Figure 3d with the other works in the literature about asbestos detection from airborne HSI datasets (see Section 2), the only study which is comparable to ours, in terms of the extension and variety of the territory considered, is Frassy et al. (2014), which covers about one half of geographical surface with respect to our case (3263 km^2 vs. 7924 km^2). Also the difference in accuracy is noteworthy (80% vs. 93% in our worst case with six classes and 98% with three classes). All the other proposals, besides considering much smaller areas, show lower performances: (Cilia et al., 2015 with an average accuracy of 86–89%, Fiumi et al., 2012 with an average accuracy of 89.1%, Fiumi et al., 2014 with an average accuracy of 75%, Szabó et al., 2014 with an accuracy of 85%, and Hamedianfar et al., 2014 with an overall accuracy of 93.42% and 88.36%).

In particular, the proposed methodology, thanks to the information assets of the hyperspectral data and the availability of the metadata about the chosen 24 municipalities, allowed a significant saving of both money and time, compared to the first survey carried out with the precise integration supplied by a drone. Indeed, while the latter has been certainly more specific and detailed, it also resulted in much more significant logistical costs and less coverage.

The results obtained for the pilot municipalities are a demonstration of how the methodology can be used on a regional scale. For this reason, as future work, the proposed procedure adopted for the search for asbestos roofings will be extended to the other municipalities in the region with a further economy of scale.

Since the wide regional territory and its difference, the idea is to periodically extend the ground truth with verified data of the new processed municipalities in order to better adapt training dataset for the third model.

Since one of the experiments has been carried out with six classes (see Section 5.2.1), it is worth noticing that the proposed architecture may be applied to HSI datasets in other scenarios (not only for binary cases of presence/absence of a material), for example, to detect other materials and/or to segment a given geographical area according to its composition in terms of vegetation, water, roads etc. (think, e.g., of construction and/or archaeological sites). Moreover, it could be interesting to study how to combine the proposed methodology with other models and datasets accounting how people move across points of interests in geographical areas like, for example, Pavan et al. (2017). Thus, local authorities could use the proposed methods to check if crowded places are at risk because of the presence of dangerous materials.

From Section 2, it clearly appears that the state-of-art method of asbestos detection (in particular for airborne HSI) is not very up to date with recent developments in machine and deep learning, still relying on classic algorithms such as SVM. Our approach goes in the direction of proposing something new, by combining three models out of a training on a large dataset, in the spirit of dynamic ensemble methods. Indeed, the choice of the third model varies from instance to instance, according to the features of the area to be classified. Of course, as explained in Section 4, the idea is based upon the dataset

exploration by GIS-domain experts, previous experiments, and repeated trials and errors. It would be interesting as a future research direction to apply novel dynamic ensemble learning algorithms like, for example, the one proposed in Alam et al. (2020), which has already been successfully applied in medical real-world classification problems. Moreover, due to the high dimensionality of HSI, a major improvement could be achieved by applying algorithms and techniques for automatic discovering and selection of feature spaces (Rafiei & Adeli, 2017), and for self-supervised learning (Rafiei et al., 2024). Finally, finite element machine approaches in the line of Pereira et al. (2020) could be explored in order to allow for real-time implementations.

ACKNOWLEDGMENTS

We thank the Regione Autonoma Friuli Venezia Giulia for having supplied the HSI dataset used in the reported experiments. This work was partially supported by the Departmental Strategic Plan (PSD) of the University of Udine – Interdepartmental Project on Artificial Intelligence (2020-25), by the Italian Minister of Defence PNRM project "Proactive Counter-UAV" (2018-2023) and by the Italian Minister of Defence PNRM project "ARGOS" (2023-2025).

REFERENCES

Abbasi, M., Mostafa, S., Vieira, A. S., Patorniti, N., & Stewart, R. A. (2022). Mapping roofing with asbestos-containing material by using remote sensing imagery and machine learning-based image classification: A state-of-the-art review. *Sustainability*, *14*(13), 8068.

Abriha, D., Kovács, Z., Ninsawat, S., Bertalan, L., Balázs, B., & Szabó, S. (2018). Identification of roofing materials with discriminant function analysis and random forest classifiers on pan-sharpened Worldview-2 imagery – A comparison. *Hungarian Geographical Bulletin*, *67*(4), 375–392. https://doi.org/10.15201/hungeobull.67.4.6

Alam, K. M. R., Siddique, N., & Adeli, H. (2020). A dynamic ensemble learning algorithm for neural network. *Neural Computing and Applications*, *32*(12), 8675–8690. https://doi.org/10.1007/s00521-019-04359-7

Blaschke, T., Hay, G. J., Kelly, M., Lang, S., Hofmann, P., Addink, E., Feitosa, R. Q., van der Meer, F., van der Werff, H., van Coillie, F., & Tiede, D. (2014). Geographic object-based image analysis – towards a new paradigm. *ISPRS Journal of Photogrammetry and Remote Sensing*, *87*, 180–191. https://doi.org/10.1016/j.isprsjprs.2013.09.014

Camera dei Deputati. (2022). La normativa in materia di amianto. https://temi.camera.it/leg18/post/OCD15_14621/la-normativa-materia-amianto.html

Cilia, C., Panigada, C., Rossini, M., Candiani, G., Pepe, M., & Colombo, R. (2015). Mapping of asbestos cement roofs and their weathering status using hyperspectral aerial images. *ISPRS International Journal of Geo-Information*, *4*(2), 928–941.

de Pinho, C. M. D., Fonseca, L. M. G., Korting, T. S., de Almeida, C. M., & Kux, H. J. H. (2012). Land-cover classification of an intra-urban environment using high-resolution images and object-based image analysis. *International Journal of Remote Sensing*, *33*(19), 5973–5995. https://doi.org/10.1080/01431161.2012.675451

Duchesne, S., Beardsell, G., Villeneuve, J.-P., Toumbou, B., & Bouchard, K. (2013). A survival analysis model for sewer pipe structural deterioration. *Computer-Aided Civil and Infrastructure Engineering*, *28*(2), 146–160. https://doi.org/10.1111/j.1467-8667.2012.00773.x

Fan, X., Zhang, X., & Yu, X. B. (2022). A graph convolution network-deep reinforcement learning model for resilient water distribution network repair decisions. *Computer-Aided Civil and Infrastructure Engineering*, *37*(12), 1547–1565. https://doi.org/https://doi.org/10.1111/mice.12813

Fiumi, L., Campopiano, A., Casciardi, S., & Ramires, D. (2012). Method validation for the identification of asbestos–cement roofing. *Applied Geomatics*, *4*(1), 55–64.

Fiumi, L., Congedo, L., & Meoni, C. (2014). Developing expeditious methodology for mapping asbestos-cement roof coverings over the territory of Lazio region. *Applied Geomatics*, *6*, 37–48.

Foresti, G. L., & Scagnetto, I. (2022). An integrated low-cost system for object detection in underwater environments. *Integrated Computer-Aided Engineering*, *29*(2), 123–139.

Frassy, F., Candiani, G., Rusmini, M., Maianti, P., Marchesi, A., Nodari, F. R., Via, G. D., Albonico, C., & Gianinetto, M. (2014). Mapping asbestos-cement roofing with hyperspectral remote sensing over a large mountain region of the Italian Western Alps. *Sensors*, *14*(9), 15900–15913.

Gamba. (2023). Pavia university (dataset). https://paperswithcode.com/dataset/pavia-university

Gibril, M. B. A., Shafri, H. Z. M., & Hamedianfar, A. (2017). New semi-automated mapping of asbestos cement roofs using rule-based object-based image analysis and Taguchi optimization technique from Worldview-2 images. *International Journal of Remote Sensing*, *38*(2), 467–491. https://doi.org/10.1080/01431161.2016.1266109

Hamedianfar, A., & Shafri, H. Z. (2014). Development of fuzzy rule-based parameters for urban object-oriented classification using very high resolution imagery. *Geocarto International*, *29*(3), 268–292. https://doi.org/10.1080/10106049.2012.760006

Hamedianfar, A., Shafri, H. Z. M., Mansor, S., & Ahmad, N. (2014). Combining data mining algorithm and object-based image analysis for detailed urban mapping of hyperspectral images. *Journal of Applied Remote Sensing*, *8*(1), 085091. https://doi.org/10.1117/1.JRS.8.085091

Hay, G. J., & Castilla, G. (2008). *Geographic Object-Based Image Analysis (GEOBIA): A new name for a new discipline* (pp. 75–89). Berlin: Springer. https://doi.org/10.1007/978-3-540-77058-9_4

Hountondji, Y., Sokpon, N., & Ozer, P. (2006). Analysis of the vegetation trends using low resolution remote sensing data in Burkina Faso (1982–1999) for the monitoring of desertification. *International Journal of Remote Sensing*, *27*(5), 871–884. https://doi.org/10.1080/01431160500382782

Hughes, G. (1968). On the mean accuracy of statistical pattern recognizers. *IEEE Transactions on Information Theory*, *14*(1), 55–63. https://doi.org/10.1109/TIT.1968.1054102

Kakarla, S. (2020). *Land cover classification of hyperspectral imagery using deep neural networks*. https://towardsdatascience.com/land-cover-classification-of-hyperspectral-imagery-using-deep-neural-networks-2e36d629a40e

Kavzoglu, T., & Mather, P. M. (2002). The role of feature selection in artificial neural network applications. *International Journal of Remote Sensing*, *23*(15), 2919–2937. https://doi.org/10.1080/01431160110107743

Krówczyńska, M., Wilk, E., Pabjanek, P., Zagajewski, B., & Meuleman, K. (2016). Mapping asbestos-cement roofing with the use of apex hyperspectral airborne imagery: Karpacz area, Poland—A case study. *Miscellanea Geographica*, *20*(1), 41–46.

Krówczyńska, M., Raczko, E., Staniszewska, N., & Wilk, E. (2020). Asbestos—cement roofing identification using remote sensing and convolutional neural networks (CNNs). *Remote Sensing*, *12*(3), 408. https://doi.org/10.3390/rs12030408

Marino, C. M., Panigada, C., & Busetto, L. (2001). Airborne hyperspectral remote sensing applications in urban areas: Asbestos concrete sheeting identification and mapping. In *IEEE/ISPRS joint workshop on remote sensing and data fusion over urban areas* (pp. 212–216). IEEE.

Myint, S. W., Gober, P., Brazel, A., Grossman-Clarke, S., & Weng, Q. (2011). Per-pixel vs. object-based classification of urban land cover extraction using high spatial resolution imagery. *Remote Sensing of Environment*, *115*(5), 1145–1161. https://doi.org/10.1016/j.rse.2010.12.017

Navulur, K. (2006). *Multispectral image analysis using the object-oriented paradigm*. CRC Press.

Neupane, B., Horanont, T., & Aryal, J. (2021). Deep learning-based semantic segmentation of urban features in satellite images: A review and meta-analysis. *Remote Sensing*, *13*(4), 808. https://doi.org/10.3390/rs13040808

Norman, M., Shafri, H. Z. M., Mansor, S., Yusuf, B., & Radzali, N. A. W. M. (2020). Fusion of multispectral imagery and Lidar data for roofing materials and roofing surface conditions assessment. *International Journal of Remote Sensing*, *41*(18), 7090–7111. https://doi.org/10.1080/01431161.2020.1754493

Olamat, A., Ozel, P., & Atasever, S. (2022). Deep learning methods for multi-channel EEG-based emotion recognition. *International Journal of Neural Systems*, *32*(05), 2250021. https://doi.org/10.1142/S0129065722500216

Ozdemir, M. A., Cura, O. K., & Akan, A. (2021). Epileptic EEG classification by using time-frequency images for deep learning. *International Journal of Neural Systems*, *31*(08), 2150026. https://doi.org/10.1142/S012906572150026X

Pavan, M., Mizzaro, S., & Scagnetto, I. (2017). *Mining movement data to extract personal points of interest: A feature based approach*, (pp. 35–61). Springer International Publishing. https://doi.org/10.1007/978-3-319-46135-9_3

Pereira, D. R., Piteri, M. A., Souza, A. N., Papa, J. P., & Adeli, H. (2020). Fema: a finite element machine for fast learning. *Neural Computing and Applications*, *32*(10), 6393–6404. https://doi.org/10.1007/s00521-019-04146-4

Raczko, E., Krówczyńska, M., & Wilk, E. (2022). Asbestos roofing recognition by use of convolutional neural networks and high-resolution aerial imagery. testing different scenarios. *Building and Environment*, *217*, 109092.

Rafiei, M. H., & Adeli, H. (2017). A new neural dynamic classification algorithm. *IEEE Transactions on Neural Networks and Learning Systems*, *28*(12), 3074–3083. https://doi.org/10.1109/TNNLS.2017.2682102

Rafiei, M. H., Gauthier, L. V., Adeli, H., & Takabi, D. (2024). Self-supervised learning for electroencephalography. *IEEE Transactions on Neural Networks and Learning Systems*, *32*(2), 2162–2388. https://doi.org/10.1109/TNNLS.2022.3190448

Regione Autonoma Friuli Venezia Giulia. (2023). Difesa dai pericoli derivanti dall'amianto. https://www.regione.fvg.it/rafvg/cms/RAFVG/ambiente-territorio/tutela-ambiente-gestione-risorse-naturali/FOGLIA44/

Sarma, H. T., & Kakarla, S. (2022). A new CNN for pixel classification in hyperspectral images. In Saraswat, M., Roy, S., Chowdhury, C., & Gandomi, A.H. (Eds.) *Proceedings of international conference on data science and applications* (pp. 773–782). Springer Singapore.

Szabó, S., Burai, P., Kovács, Z., Szabó, G., Kerényi, A., Fazekas, I., Paládi, M., Buday, T., & Szabó, G. (2014). Testing algorithms for the identification of asbestos roofing based on hyperspectral data. *Environmental Engineering and Management Journal*, *143*(11), 2875–2880.

Taherzadeh, E., & Shafri, H. (2013). Development of a generic model for the detection of roof materials based on an object-based approach using Worldview-2 satellite imagery. *Advances in Remote Sensing*, *2*(4), 312–321.

Tommasini, M., Bacciottini, A., & Gherardelli, M. (2019). A QGIS tool for automatically identifying asbestos roofing. *ISPRS International Journal of Geo-Information*, *8*(3), 131. https://doi.org/10.3390/ijgi8030131

How to cite this article: Gubiani, D., Sgrazzutti, G., Basso, M., Viero, E., Tavaris, D., Foresti, G. L., & Scagnetto, I. (2024). A dynamic neural network model for the identification of asbestos roofings in hyperspectral images covering a large regional area. *Computer-Aided Civil and Infrastructure Engineering*, 1–16. https://doi.org/10.1111/mice.13376